



**HAL**  
open science

## Measles virus-imposed remodeling of the autophagy machinery determines the outcome of bacterial coinfection

Mathieu Claviere, Aude Lavedrine, Guénaëlle Lamiral, Mariette Bonnet, Pauline Verlhac, Denitsa S Petkova, Lucile Espert, Rémi Duclaux-Loras, Julie Lucifora, Michel Rivoire, et al.

► **To cite this version:**

Mathieu Claviere, Aude Lavedrine, Guénaëlle Lamiral, Mariette Bonnet, Pauline Verlhac, et al.. Measles virus-imposed remodeling of the autophagy machinery determines the outcome of bacterial coinfection. *Autophagy*, 2022, pp.1 - 15. 10.1080/15548627.2022.2107309 . hal-03845891

**HAL Id: hal-03845891**

**<https://hal.science/hal-03845891>**

Submitted on 9 Nov 2022

**HAL** is a multi-disciplinary open access archive for the deposit and dissemination of scientific research documents, whether they are published or not. The documents may come from teaching and research institutions in France or abroad, or from public or private research centers.

L'archive ouverte pluridisciplinaire **HAL**, est destinée au dépôt et à la diffusion de documents scientifiques de niveau recherche, publiés ou non, émanant des établissements d'enseignement et de recherche français ou étrangers, des laboratoires publics ou privés.




# Measles Virus-Imposed Remodeling of the Autophagy Machinery Determines the Outcome of Bacterial Coinfection

Mathieu Claviere, Aude Lavedrine, Guénaëlle Lamiral, Mariette Bonnet, Pauline Verlhac, Denitsa S. Petkova, Lucile Espert, Rémi Duclaux-Loras, Julie Lucifora, Michel Rivoire, Gilles Boschetti, Stéphane Nancey, Aurore Rozières, Christophe Viret & Mathias Faure


To cite this article: Mathieu Claviere, Aude Lavedrine, Guénaëlle Lamiral, Mariette Bonnet, Pauline Verlhac, Denitsa S. Petkova, Lucile Espert, Rémi Duclaux-Loras, Julie Lucifora, Michel Rivoire, Gilles Boschetti, Stéphane Nancey, Aurore Rozières, Christophe Viret & Mathias Faure (2022): Measles Virus-Imposed Remodeling of the Autophagy Machinery Determines the Outcome of Bacterial Coinfection, *Autophagy*, DOI: [10.1080/15548627.2022.2107309](https://doi.org/10.1080/15548627.2022.2107309)

To link to this article: <https://doi.org/10.1080/15548627.2022.2107309>

 View supplementary material 

 Accepted author version posted online: 28 Jul 2022.

 Submit your article to this journal 

 Article views: 13

 View related articles 

 View Crossmark data 

**Publisher:** Taylor & Francis & Informa UK Limited, trading as Taylor & Francis Group

**Journal:** *Autophagy*

**DOI:** 10.1080/15548627.2022.2107309

**Measles Virus-Imposed Remodeling of the Autophagy Machinery Determines the Outcome of Bacterial Coinfection**

Mathieu Clavier<sup>1,#</sup>, Aude Lavedrine<sup>1,#</sup>, Guénaëlle Lamiral<sup>1</sup>, Mariette Bonnet<sup>1</sup>, Pauline Verlhac<sup>1</sup>, Denitsa S. Petkova<sup>1</sup>, Lucile Espert<sup>2</sup>, Rémi Duclaux-Loras<sup>1,3</sup>, Julie Lucifora<sup>1</sup>, Michel Rivoire<sup>4</sup>, Gilles Boschetti<sup>1,5</sup>, Stéphane Nancey<sup>1,5</sup>, Aurore Rozières<sup>1</sup>, Christophe Viret<sup>1,\*</sup> and Mathias Faure<sup>1,6,\*°</sup>

<sup>1</sup>CIRI, Centre International de Recherche en Infectiologie, Université de Lyon, Inserm U1111, Université Claude Bernard Lyon 1, CNRS, UMR5308, ENS de Lyon, F-69007, Lyon, France.

<sup>2</sup>IRIM, University of Montpellier, UMR 9004 CNRS, Montpellier, France

<sup>3</sup>Department of Pediatric Hepatology, Gastroenterology and Nutrition, Femme-Mère-Enfant Hospital, Hospices Civils de Lyon, Bron, France.

<sup>4</sup>Inserm U1032, Centre Léon Bérard (CLB), Lyon, France.

<sup>5</sup>Department of Gastroenterology, Lyon-Sud university hospital, Hospices Civils de Lyon, Lyon, France

<sup>6</sup>Equipe Labellisée par la Fondation pour la Recherche Médicale, FRM

#Equal contribution

\*Equal contribution

°Corresponding author: [mathias.faure@inserm.fr](mailto:mathias.faure@inserm.fr) ; CIRI, INSERM U1111, CNRS UMR 5308, ENS-L, UCBL1 - 21, Avenue Tony Garnier 69365 Lyon Cedex 07, France. Phone: +33-4-37-28-23-42

## Abstract

Although it is admitted that secondary infection can complicate viral diseases, the consequences of viral infection on cell susceptibility to other infections remain underexplored at the cellular level. We thought to examine whether the sustained macroautophagy/autophagy associated with measles virus (MeV) infection could help cells oppose invasion by *Salmonella* Typhimurium, a bacterium sensitive to autophagic restriction. We report here the unexpected finding that *Salmonella* markedly replicated in MeV-infected cultures due to selective growth within multinucleated cells. Hyper-replicating *Salmonella* localized outside of LAMP1-positive compartments to an extent that equaled that of the predominantly cytosolic *sifA* mutant *Salmonella*. Bacteria were subjected to effective ubiquitination but failed to be targeted by LC3 despite an ongoing productive autophagy. Such a phenotype could not be further aggravated upon silencing of the selective autophagy regulator TBK1 or core autophagy factors ATG5 or ATG7. MeV infection also conditioned primary human epithelial cells for augmented *Salmonella* replication. The analysis of selective autophagy receptors able to target *Salmonella* revealed that a lowered expression level of SQSTM1/p62 and TAX1BP1/T6BP autophagy receptors prevented effective anti-*Salmonella* autophagy in MeV-induced syncytia. Conversely, as SQSTM1/p62 is promoting the cytosolic growth of *Shigella flexneri*, MeV infection led to reduced *Shigella* replication. The results indicate that the rarefaction of dedicated autophagy receptors associated with MeV infection differentially affects the outcome of bacterial coinfection depending on the nature of the functional relationship between bacteria and such receptors. Thus, virus-imposed reconfiguration of the autophagy machinery can be instrumental in determining the fate of bacterial coinfection.

**Keywords:** autophagy, bacteria, co-infection, syncytia, virus

**Abbreviations:** ACTB/ $\beta$ -ACTIN: actin beta; ATG: autophagy related; BAFA1: bafilomycin A<sub>1</sub>; CFU: colony-forming units; CALCOCO2/NDP52: calcium binding and coiled-coil domain 2; FIP: fusion inhibitory peptide; GFP: green fluorescent protein; LAMP1: lysosomal associated membrane

protein 1; LIR: MAP1LC3/LC3-interacting region; MAP1LC3/LC3: microtubule associated protein 1 light chain 3; MeV: measles virus; MOI: multiplicity of infection; OPTN: optineurin; PHH: primary human hepatocyte; SCV: Salmonella-containing vacuoles; SQSTM1/p62: sequeosome 1; *S. flexneri*: *Shigella flexneri*; *S. Typhimurium*: *Salmonella enterica* serovar Typhimurium; TAX1BP1/T6BP: Tax1 binding protein; TBK1: TANK binding kinase 1

ACCEPTED MANUSCRIPT

## INTRODUCTION

Macroautophagy/autophagy is a highly conserved cellular process that contributes to cell homeostasis via the degradation and recycling of cytosolic components. It relies on the formation of membrane elements, or phagophores, that evolve into double-membrane vesicles named autophagosomes to encapsulate cytosolic materials and direct them to the endo-lysosomal pathway for degradation, a process that involves dozens of ATG (autophagy related) proteins [1,2]. Developing phagophores can selectively target particular cytosolic cargoes due to engagement of dedicated factors called selective autophagy receptors [3,4]. Such receptors interact in a ubiquitin-dependent or -independent manner, with given cargoes on the one hand and with phagophore-anchored Atg8-family proteins, such as lipidated MAP1LC3/LC3 (microtubule associated protein 1 light chain 3), on the other hand [5]. Apart from endogenous cargoes to be recycled, autophagy can target microorganisms that invade the cytosol. Perhaps, the best evidence for autophagy being a powerful cell-autonomous defense mechanism is the fact that many intracellular pathogens have evolved strategies to avoid, oppose or manipulate the autophagy machinery [6,7]. Autophagy can help to resist viral infections by promoting induction of type-I interferons or selectively degrading viral components. In turn, viruses may escape or subvert autophagy to promote their life cycle [8,9]. In the case of the measles virus (MeV), infection rapidly initiates a transient phase of autophagic activity and, after a return to baseline level, activates a sustained second wave associated with viral protein synthesis and virus replication [10-12]. The latter wave that benefits to the virus is further promoted by fusion events associated with the formation of multinucleated cells (syncytia) [11,13,14]. CALCOCO2/NDP52 and TAX1BP1/T6BP autophagy receptors promote MeV replication while SQSTM1/p62 harbors a rather anti-viral function [15]. Autophagy can also oppose intracellular bacterial infections (xenophagy) as exemplified by *Salmonella enterica* Serovar Typhimurium (*S. Typhimurium*). In infected epithelial cells, *Salmonella* are initially confined into Salmonella-containing vacuoles (SCVs). Some bacteria become cytosolic due to SCV damaging by the type 3 secretion system (T3SS). Both ubiquitinated cytosolic bacteria and damaged SCVs get rapidly targeted by autophagy receptors. The targeting can involve CALCOCO2, SQSTM1, OPTN (optineurin) and TAX1BP1 [16-21]. As a substantial knowledge on

the interaction of both MeV and *S. Typhimurium* with the autophagy machinery of epithelial cells is available, we used it as a frame to explore the outcome of MeV and *S. Typhimurium* co-infection experiments in terms of autophagic activity, pathogen sensing and pathogen fate. We anticipated that *S. Typhimurium* might be more efficiently detected and degraded in MeV-infected than in non-infected cells. Surprisingly, *S. Typhimurium* could in fact massively replicate in virus-bacteria co-infected cells despite MeV-induced sustained autophagic activity. This phenotype relied on MeV infection-associated changes in the autophagy machinery that could also modify the host cell susceptibility to another invading bacterium.

ACCEPTED MANUSCRIPT

## RESULTS

### *S. Typhimurium hyper-replicates in MeV-induced syncytia.*

The MeV is a prototypical example of viruses capable of initiating a marked and sustained autophagic activity characterized by a complete flux that benefits to, and is required for, its optimal replication [10-12,15,22]. To examine the fate of a pathogen known to be sensitive to autophagic degradation when it enters cells harboring an enhanced, pathogen-induced, autophagic activity, we used *S. Typhimurium* to infect cultures previously infected with MeV. HeLa epithelial cells infected with MeV for 48 h and exposed to *S. Typhimurium* were studied after 6 h of co-infection. When analyzing the status of LC3 by immunoblot, we observed that MeV and *S. Typhimurium* co-infected cultures were characterized by an augmented level of LC3 lipidation (**Figure 1A**). Concerning bacteria growth, we found that, relative to virus-free cultures, MeV and *S. Typhimurium* co-infected cultures, where 60 to 75% of the nuclear mass corresponded to syncytial cells (not shown), displayed a marked replication of the bacteria (**Figure 1B**). To document this exacerbated growth by a distinct approach, we numbered bacteria on monolayer of MeV and *S. Typhimurium* co-infected cells after immunostaining for both pathogens and confocal microscopy analysis. We found again that *S. Typhimurium* hyper-replicated in co-infected cells as evidenced by the presence of areas occupied by large patches of accumulating bacteria. Bacteria growth was unlikely to be due to an augmented internalization rate into MeV-infected cells because MeV-infected and uninfected cultures showed similar bacterial growth up to 4 h after co-infection. Remarkably, *Salmonella* hyper-replication was taking place selectively within syncytia, the multinucleated giant cells that result from multiple rounds of fusion between MeV-infected cells and uninfected neighboring cells (**Figure 1C**). In term of kinetics, the replicative burst was clearly occurring between 4 h and 6 h post *S. Typhimurium* infection (**Figure 1D**).

To further evaluate the importance of syncytia formation in the hyper-replication of *S. Typhimurium*, HeLa cells were cultured in the presence of a recombinant fusion inhibitory peptide (FIP) that blocks the formation of syncytia without interfering with the entry of the virus into host cells [23]. Interestingly, under such a condition, we failed to detect *S. Typhimurium* hyper-replication in the co-infected culture analyzed by gentamycin protection assay (**Figure 1E**) as well as in co-



infected cells examined individually by confocal microscopy (**Figure 1F**). As sustained autophagy is also observed within syncytia generated by using HeLa cells only transfected with both MeV-F and MeV-H proteins [11], we also examined the fate of *S. Typhimurium* in MeV-F- and MeV-H-induced syncytia and found again that relative to control cells, *S. Typhimurium* replication was favored with patches of bacteria selectively accumulating in multinucleated cells (**Figure S1A and S1B**).

These results indicate that, despite its associated active autophagy flux, MeV infection conditioned HeLa epithelial cell cultures for enhanced proliferation of invading Salmonella and that such a hyper-replication was selectively associated with syncytial cells. The recapitulation of Salmonella hyper-replication in MeV-F and MeV-H-induced syncytia indicated that viral replication itself was not instrumental for bacterial growth.

***S. Typhimurium hyper-replicates in MeV-induced syncytia outside of LAMP1-positive vesicles and is not targeted to phagophores despite effective ubiquitination.***

*S. Typhimurium* can be targeted for autophagic degradation either at the step of SCV rupture that is sensed through detection of newly exposed carbohydrates or, when it becomes ubiquitinated following exit from the vacuole [16,18,20]. We thus asked whether bacteria that accumulated within MeV-induced syncytia could escape active autophagy due to confinement within particular compartments such as the SCV that forms within epithelial cells. To this end, we examined MeV and *S. Typhimurium* co-infected syncytia for the distribution of hyper-replicative bacteria relative to that of vacuolar compartments that stain positive for LAMP1 (lysosomal-associated membrane protein 1), a factor actively recruited to SCVs [24]. As expected, we could reliably detect colocalization of bacteria with LAMP1-positive membranes in HeLa cells infected with bacteria only, and such colocalization events were clearly less frequent in the case of the *sifA* mutant bacteria known to be predominantly cytosolic [25,26] (**Figure 2A**). Strikingly, when looking at syncytia from MeV and *S. Typhimurium* co-infected cultures, we found that hyper-replicating bacteria were poorly associated with LAMP1-positive compartments, with a level of colocalization closely resembling that observed for syncytia supporting the hyper-replication of *sifA* mutant bacteria (**Figure 2A**). Consistent with this result, we observed that after 2 h of infection, mononuclear cells and MeV-F and MeV-H-induced syncytia

displayed comparable levels of bacteria/LAMP1 colocalization and that after 6 h, this colocalization dropped in the case of MeV-F and MeV-H syncytial cells (**Figure S1C**). Because it remained possible that bacteria accumulating in MeV-induced syncytia were confined within unusual vacuolar compartments that were negative for LAMP1 expression, we processed the cultures for analysis by transmission electron microscopy. We observed that, in contrast to HeLa cells infected with *S. Typhimurium* only, in which bacteria were frequently surrounded by membranes, bacteria that accumulated within multinucleated cells were devoid of vesicular membrane in their immediate vicinity and thereby, resembled those seen in multinucleated cells infected with the *sifA* mutant strain (**Figure 2B**).

Given that the autophagy that characterizes MeV-induced syncytial cells appears not to oppose the cytosolic growth of *S. Typhimurium*, we wondered whether the targeting of *S. Typhimurium* by the autophagy machinery was operating normally. Within the cytosol of normal epithelial cells, *S. Typhimurium* cells are typically coated with ubiquitin tags that are recognized by autophagy receptors, which themselves interact with LC3 factors anchored on the growing phagophore [18]. We therefore examined the status of bacteria within syncytia in terms of colocalization with both ubiquitin and LC3. Well consistent with their cytosolic localization documented above, we found that a majority of bacteria that replicated within syncytia were efficiently ubiquitinated. In contrast, only a very limited fraction of bacteria could effectively colocalize with LC3 within syncytia (**Figure 2C**). As the experiment was performed with HeLa cells stably expressing GFP-LC3, we inferred that *Salmonella* hyper-replication was not related to an insufficient supply in the core autophagy factor LC3. Thus, within the cytosolic microenvironment of MeV-induced syncytia, *S. Typhimurium* successfully escaped autophagosomal targeting despite being efficiently tagged by the ubiquitination machinery. Most notably, LC3 failed to be recruited to ubiquitinated *S. Typhimurium*.

***TBK1 regulator and the ATG5 and ATG7 core autophagy factors fail to regulate the growth of S. Typhimurium in MeV-induced syncytial cells.***

Because TBK1 (TANK binding kinase 1) is an important serine/threonine kinase that regulates the engagement of several autophagy receptors involved in the xenophagic response to *S. Typhimurium*

infection [17,27,28], we evaluated whether endogenous TBK1 was supporting a certain level of xenophagic response to *S. Typhimurium* in syncytial cells. When regular HeLa cells were treated with the TBK1 activity inhibitor BX795 [29] at the time of *S. Typhimurium* infection, we could detect, as expected, an increase in the average number of bacteria per nucleated cells (**Figure 3A**). By contrast, in MeV-induced syncytia co-infected with *S. Typhimurium*, the presence of BX795 did not cause any detectable augmentation of the bacterial load relative to vehicle-treated cells (**Figure 3A**), despite the fact that BX795 did not alter the expression level of TBK1 (**Figure S2A**). Separate experiments where TBK1 expression was impaired by using small interfering (si)RNA treatment revealed consistent results: unlike in co-infected mononucleated cells, lowering the expression of TBK1 failed to modulate bacteria growth in MeV-induced syncytia (**Figure 3B and Figure S2B**).

To examine whether autophagy at large can regulate *S. Typhimurium* growth to some extent in MeV co-infected cells, we used HeLa cells that were previously treated with siRNAs to silence the expression of the core autophagy factors ATG5 and ATG7. We first observed that the high level of LC3 lipidation that was induced by MeV, and persisted upon *S. Typhimurium* co-infection, remained readily dependent on both ATG5 and ATG7 (**Figure S3A-B**). Strikingly, when bacteria replication was examined in these cells, we found that deficiency in either ATG5 or ATG7 did not modify the growth of *S. Typhimurium* in co-infected cells relative to cells treated with control siRNAs (**Figure 3C**). Thus, as ATG5 and ATG7 silencing experiments did not further aggravate *S. Typhimurium* growth, they revealed that the capacity of MeV-induced syncytia to mount an anti-Salmonella xenophagic response was already entirely exhausted.

***The sustained autophagic activity associated with MeV infection leads to exacerbated degradation of SQSTM1 and TAX1BP1 autophagy receptors.***

Because enrichment in LC3-II can be observed under circumstances where autophagosomes are readily induced but do not efficiently mature into autolysosomes, we wondered whether the marked LC3 lipidation activity detectable under conditions of co-infection was associated with an effective degradative activity. We thus examined the fate of SQSTM1, a long-lived protein that is normally catabolized by autophagy and whose degradation serves as an indicator for the completion of the

autophagy flux [30]. We observed that co-infection of MeV-infected cultures with *S. Typhimurium* did not interfere with the efficient degradation of SQSTM1 (**Figure 4A**), indicating that under such conditions, the autophagic activity remained fully degradative. Thus, in MeV-infected cultures where syncytial cells form and grow, secondary infection with *S. Typhimurium* interfered neither with LC3 lipidation nor the degradative potential of the pre-existing autophagy flux. Besides the marked SQSTM1 degradation seen MeV-infected cells [11,22], we examined the expression status of *Salmonella*-relevant selective autophagy receptors in MeV-infected cells and found that while CALCOCO2 and OPTN expression level remained virtually unchanged, TAX1BP1 level was diminished as well (**Figure 4B**). The remodeling of the autophagy receptor expression pattern was not due to autophagy receptor degradation by viral proteases because the MeV genome does not encode such enzymes and because this reduction was also observed in MeV-F and MeV-H-induced syncytia (**Figure S3C**). To gain further insight into the lowered expression of SQSTM1 and TAX1BP1 autophagy receptors in MeV-infected cells, we monitored their expression level, along with the status of LC3, in the presence of bafilomycin A<sub>1</sub> (BAFA1) or MG132 inhibitors in order to delineate their dependency on autophagic versus proteasomal degradative pathways (**Figure 4C**). While TAX1BP1 was partially dependent on proteasomal degradation at steady state, both SQSTM1 and TAX1BP1 expression levels were markedly upregulated when MeV-infected cells were exposed to BAFA1, indicating that their augmented degradation involved autophagy. Co-infecting cells with *S. Typhimurium* did not aggravate, or antagonize, the changes imposed by MeV infection on SQSTM1 and TAX1BP1 receptor expression. With respect to LC3 lipidation, its magnitude was strongly augmented in the presence of BAFA1 relative to control cultures in all settings analyzed, implying that coinfection with *S. Typhimurium* did not abrogate the autophagic activity induced by MeV infection. Collectively, the results point to an overconsumption of both SQSTM1 and TAX1BP1 autophagy receptors in MeV-infected cells as a consequence of the autophagic activity induced by the virus.

***The enforced expression of SQSTM1 and TAX1BP1 autophagy receptors restores the capacity of MeV infected cells to mount an anti-Salmonella autophagic response.***

Reasoning that a lowered expression level of autophagy receptors in syncytia might substantially compromise *Salmonella* targeting and favor bacteria hyper-replication, we asked what would be the fate of *Salmonella* infection when host cells harbor a stabilized expression of the relevant autophagy receptors before co-infection with MeV and *Salmonella*. We stably expressed SQSTM1 or TAX1BP1 in HeLa cells prior to co-infection experiments (**Figure S4A**). Colony-forming units (CFU) assay analysis revealed that, relative to cultures transfected with an empty vector, MeV-infected cultures derived from cells engineered to express either SQSTM1 or TAX1BP1 revealed an augmented capacity to resist *Salmonella* intracellular replication (**Figure 5A**). Along the same line, MeV-induced syncytia from cultures with enforced SQSTM1 or TAX1BP1 expression harbored a reduced level of *Salmonella* replication as assessed by the direct numeration of bacteria 6 h post-infection (**Figure 5B**). This effect was not caused by a change in susceptibility to MeV infection because the number and size of formed syncytia were comparable in all conditions (not shown).

Because SQSTM1 possesses multiple protein domains able to interact with various partners and is, for instance, capable of activating the transcription factor NF $\kappa$ B/NF- $\kappa$ B [31,32], we investigated whether the restriction of *Salmonella* we observed in SQSTM1-overexpressing syncytia, effectively involved a role for the autophagy receptor function of SQSTM1. We thus performed a separate complementation experiment to compare the effect of WT SQSTM1 and a mutant form of SQSTM1 that is unable to interact with LC3, due to deletion of its LC3-interacting region (LIR) motif (SQSTM1 $\Delta$ LIR), and therefore unable to fulfill its selective autophagy receptor function [33,34]. Importantly, we found that, SQSTM1 $\Delta$ LIR failed to restore the capacity of syncytial cells to restrict *Salmonella* growth (**Figure 5C**). We conclude that, in MeV-induced syncytia, the capacity of ectopically expressed SQSTM1 to restrict *Salmonella* replication requires a SQSTM1-LC3 interaction and therefore, effectively relies on the autophagy receptor function of SQSTM1. When we examined the colocalization of bacteria with LC3 within syncytia, we found that the provision of either SQSTM1 or TAX1BP1 receptor augmented the targeting of *Salmonella* by LC3 and that, in the case of SQSTM1, this effect was sensitive to mutation affecting the LIR motif (**Figure 5D**). When the analysis was performed at the early time point of 30 min after *Salmonella* infection, similar restoration

effects were observed with the additional observation that in control cells (empty vector) the targeting of bacteria by LC3 was quite comparable between 30 min and 6 h after infection, suggesting that in MeV-infected cells, *Salmonella* targeting by autophagy is already not very efficient early after infection (**Figure S4B**). Finally, SQSTM1 or TAX1BP1 overexpression also improved the colocalization of bacteria with the lysosomal marker LAMP1 in MeV-induced syncytia (**Figure 5E** and **S4C**). Altogether, the results indicate that, during MeV infection, the expression level of dedicated autophagy receptors can represent a checkpoint for the capacity of host cells to mount an efficient autophagic response against *Salmonella* invasion.

***MeV infection conditions human primary epithelial cells for S. Typhimurium cytosolic hyper-replication.***

To determine whether the observations obtained with HeLa cells could be valid for primary epithelial cells, we used primary epithelial cells derived from healthy portions of liver biopsies from two patients undergoing partial hepatectomy. For both donors, we observed hyper-replication of *Salmonella* in MeV and *Salmonella* co-infected primary hepatocyte cultures relative to control cultures infected with *Salmonella* only (**Figure 6A**). In agreement with results from the CFU assay, accumulating bacteria could be clearly visualized by confocal microscopy in syncytial cells of MeV and *Salmonella* co-infected primary hepatocyte cultures (**Figure 6B**). Finally, we could also detect a marked reduction in SQSTM1 expression in primary hepatocytes upon infection with MeV (**Figure 6C**). Hence, the influence of MeV infection on the capacity of host cells to restrict bacterial growth upon *Salmonella* co-infection can be observed for primary epithelial cells as well.

***MeV infection renders HeLa cells more resistant to Shigella flexneri intracellular growth.***

In order to test whether MeV infection could influence the outcome of secondary infection with an invasive bacterium distinct from *S. Typhimurium*, we performed similar experiments with *Shigella flexneri*. In sharp contrast with experiments performed with *S. Typhimurium*, we observed that MeV infection significantly reduced the ability of *S. flexneri* to replicate in the cytosol of co-infected HeLa cells (**Figure 6D**). Although this result could have seemed counter-intuitive, it actually constitutes a

confirmation of the negative influence of MeV infection on the homeostasis of the SQSTM1 autophagy receptor because the cytosolic growth of *S. flexneri* in HeLa cells was reported to be dependent on the level of SQSTM1 [35]. Thus, SQSTM1 overconsumption associated with MeV-induced autophagy can differentially impact the cytosolic growth of invading bacteria depending on the functional relationship that evolved between these bacteria and SQSTM1.

## DISCUSSION

The anti-microbial potential of autophagy is well studied in the context of individual infection, and various active molecular mechanisms evolved by individual pathogens to counteract or hijack autophagy have also been described [36-38]. Much less effort has been made to examine the anti-microbial autophagic potential of cells exposed to more than one pathogen. Here, by exploring for the first time, anti-microbial autophagy under conditions of co-infection in epithelial cells, we characterized a not yet appreciated mechanism of xenophagy escape. We identified virus-induced selective autophagy receptor exhaustion as a major driving force weakening anti-*Salmonella* autophagy in co-infected cells, a phenomenon that may constitute a strong susceptibility factor for some opportunistic bacterial infections.

We found that the autophagy sensitive *S. Typhimurium* bacterium hyper-replicates in MeV-infected cells, despite the occurrence of an intense and sustained autophagic activity. This unexpected massive replication selectively takes place within the cytosol of virus-induced multinucleated cells. While bacteria are efficiently ubiquitinated, they are clearly not subjected to efficient targeting by the autophagy machinery. The extent of bacterial growth was indeed comparable to that observed when hosts cells had impaired autophagic activity due to silencing of ATG5 or ATG7 core autophagy factors. Among autophagy factors whose amount is crucial for efficient anti-bacterial selective autophagy are autophagy receptors. Indeed, the experimentally reduced level of a single of the relevant autophagy receptors is sufficient to weaken the autophagic restriction of *Salmonella* [17-19,39] and both SQSTM1 and TAX1BP1 are important for the autophagic targeting of ruptured SCVs in mammalian cells [40]. Reduction in autophagy factors levels could be due to their marked and continuous degradation in relation with the ongoing sustained autophagy that characterizes MeV-

induced syncytia. In line with this possibility, we found that SQSTM1 and TAX1BP1 expression levels are lowered, in a bafilomycin-dependent manner, in co-infected cultures and, are also reduced in MeV-F and MeV-H-induced syncytia. In addition, MeV infection-associated reduction in SQSTM1 expression was also seen in primary human epithelial cells. Strikingly, the single overexpression of TAX1BP1 or, of an autophagy-competent form of SQSTM1, was sufficient to restore a restrictive pressure on intra-syncytial *S. Typhimurium* growth. Thus, the exacerbated autophagic degradation of autophagy receptors appears to be the main mechanism by which MeV-infection compromises subsequent anti-bacterial autophagy in syncytia. Keeping SQSTM1 level low is certainly beneficial for MeV since this autophagy receptor appears capable of anti-MeV activity [15]. The results emphasize that the level of SQSTM1 expression appears to be crucial to calibrate an efficient anti-*Salmonella* autophagic response. Autophagy receptors have the unique properties to induce autophagosome formation upon cargo recognition, to target pathogens towards growing autophagosomal membranes, and eventually to regulate the fusion of pathogen-containing autophagosomes with the endo-lysosomal compartments for cargo degradation [17,41-43]. Following cargo-binding, SQSTM1 is able to initiate autophagosome formation by interacting with FIP200, a member of the ULK1 complex [44], and can recruit TBK1 for an efficient autophagosomal uptake of ubiquitinated cargoes [45]. We found that unlike in mononuclear cells, TBK1 activity cannot influence the fate of bacteria in syncytia, a result well compatible with the notion of a defective targeting of *S. Typhimurium* by the autophagy machinery. Interestingly, TBK1 recruitment to SQSTM1-containing aggregates could involve TAX1BP1 [46]. Thus, beyond binding to ubiquitinated *Salmonella* to target it to degradation [21], the lowered level of TAX1BP1 in MeV-induced syncytia could also contribute to *Salmonella* escape from xenophagy via dysfunctional autophagy receptor regulation.

Syncytia are incompletely understood cellular entities and one cannot exclude that additional, non-mutually exclusive effects may contribute in some extent to the defective autophagic targeting of *Salmonella*. The *Salmonella* ubiquitination pattern in syncytial cells could qualitatively differ from that occurring in mononucleated epithelial cells, what could modulate the interaction of ubiquitin-binding domains (UBDs) of autophagy receptors with ubiquitin chains on bacteria [19,39,47,48]. It could also be possible that MeV-infection inhibits the functioning of certain autophagy factors



required for the proper targeting of *Salmonella*. MeV factors able to interact with autophagy factors could compete with cellular partners of these factors that are important for cargo targeting, as seen in other viral infection contexts [15,49-51]. Finally, the targeting of *Salmonella* by the autophagy machinery of syncytia could be less efficient due to delocalization of necessary factors. Such localized deprivations could rely on a discontinuous distribution of these factors within the intra-syncytial space in relation with the ongoing autophagy that is induced and utilized by the virus to promote its replication [52-54], and/or with the requirement for syncytial homeostasis.

Components of the autophagy machinery can participate in repairing the damage that the bacterial type 3 secretion system can cause to the SCV, thereby promoting bacteria survival/growth within the vacuole [55]. How autophagy proteins exactly proceed to repair ruptured vacuoles is currently not elucidated. It is also not known whether autophagy receptors play any role in this repair. If such a repair is altered upon infection with MeV or involve a role for SQSTM1 and/or TAX1BP1, we assume it could contribute to the release of *Salmonella* into the cytosol and promote their hyper-replication by favoring the exit of bacteria.

When examining the magnitude of *S. flexneri* growth within epithelial cell cultures infected with MeV, we observed that instead of promoting the intracellular replication of the bacteria, MeV infection significantly attenuated it. This result was well consistent with the observation of SQSTM1 autophagy receptor augmented degradation in MeV-infected cells because SQSTM1 was in fact reported as a facilitating factor for *Shigella* growth in epithelial cells by Mostowy and colleagues [56]. Thus, depending on the functional relationship that evolved between invasive bacteria and the SQSTM1 autophagy receptor, SQSTM1 augmented degradation associated with MeV infection can either promote or restrict the intracellular growth of invading bacteria.

In conclusion, our results indicate that within the cytosol of syncytia associated with MeV infection, quantitative variations in cognate autophagy receptors allow *Salmonella* to outcompete anti-bacterial selective autophagy response. As they stand, the results identify virus-induced reconfiguration of the autophagy receptor repertoire as a cell-autonomous feature that is likely to contribute to the susceptibility to some super-infections, especially in infectious disease associated with pathogen-

induced syncytial cells. As secondary infections are an important source of complication/mortality during infection, including measles [57-60], and because syncytia formation is rather frequent during infection by enveloped viruses, we suggest that modifications of the anti-microbial selective autophagic potential of host epithelial cells should be considered with respect to opportunistic additional-infections in virally infected patients.

## **MATERIALS AND METHODS**

### ***Cell lines, antibodies, and reagents***

Human cervix carcinoma epithelial cells (HeLa; ATCC, CRM-CCL-2) and HeLa cells stably expressing the GFP-LC3 reporter construct were maintained in Dulbecco's Modified Eagle Medium (DMEM; Gibco, 61965026) complemented with 10% fetal bovine serum (FBS), 50 µg/mL gentamicin. The antibodies used for western blot (WB) and Immunofluorescence analysis (IF) were the following: anti-LC3B (Sigma, L7543) WB 1:1000; anti-SQSTM1/p62 (Santa Cruz Biotechnology, sc-28359) WB 1:1000; anti-MeV-N (mouse monoclonal clone 120) Mathias Faure laboratory, WB and IF 1:1000, anti-ATG5 (Sigma, A0866) WB 1:1000, anti-ATG7 (Sigma, AZ836) WB 1:1000, ACTB/β-ACTIN (Cell Signaling Technology, 12262) WB 1:1000, anti-GAPDH (Ozyme, 14C10) WB 1:1000, anti-TBK1 (Santa Cruz Biotechnology, sc- 9912,) WB 1:1000, anti-rabbit IgG HRP (Sigma, A05045) WB 1:5000, anti-mouse IgG HRP (Invitrogen, 626520), anti-goat IgG HRP (Thermo Scientific, 51402) WB 1:5000, anti-*Salmonella* LPS (Thermo Scientific, PA1-7244) WB 1:2000, anti-LAMP1 (CD107a; BD Pharmingen, 555798) IF 1:200, anti-Ubiquitin (Millipore, clone FK2; 04-263) IF 1:1000, Alexa Fluor 549 anti-rabbit IgG (Jackson ImmunoResearch, 111-505-047), and Alexa Fluor 647 anti-mouse IgG (Jackson ImmunoResearch, 715-605-150) IF 1:1000. Pharmacological reagents used were BX795 1 mM (Sigma, 702675-74-9), BAFA1 (50 nM) and MG132 (10 nM) inhibitors (Sigma, 88899-55-2 and 133407-82-6, respectively) and the fusion inhibitory FIP peptide (10 µg/mL; Sigma, C9405; Z-D-Phe-L-Phe-Gly-OH).

### ***Primary human hepatocytes (PHH)***

PHH were freshly prepared from human liver resections obtained from the Centre Léon Bérard (Lyon) with French ministerial authorizations (AC 2013-1871, DC 2013 – 1870, AFNOR NF 96 900 sept 2011) as previously described<sup>61</sup>. PHH cultures were used 2-3 days after seeding for MeV infection at MOI of 0.03 pfu/cell. Infected PHH and corresponding controls were kept for 48 h.

### ***Cell transfection***

The day before transfection, 105 cells were seeded in 6-well plates in OPTIMEM medium (Gibco, 31985047) supplemented with 10% FBS, 0.1% gentamicin, 0.1 mM non-essential amino acids (Gibco, 11140035), 1 mM sodium pyruvate, 0.1 g/L sodium bicarbonate. Cells were transfected with 100 pmol of siRNA targeting *ATG5* or *ATG7* or *TBK1* (Dharmacon) using Lipofectamine RNAiMAX (Invitrogen, 13778030) following the manufacturer's instructions. Cells were eventually co-transfected with a mix of 500 ng of each of the plasmids pCXN2-F (Edmonston strain) and pCXN2-H (Edmonston strain) [11], both kindly provided by Dr Y. Yanagi (Kyushu university, Fukuoka, Japan), using Dreamfect gold (OZ Biosciences, DG80500) following the manufacturer's instruction. Twenty-four h post transfection, MeV-F and MeV-H expression were checked by FACS analysis of cell suspensions using clone 55 and Y503 specific mouse monoclonal antibodies, respectively (Mathias Faure Laboratory).

### ***Western blot***

Cells were lysed using 0.5% Nonidet P40 (Roche, 11754599001) supplemented with complete protease inhibitor (Roche, 11836153001) in PBS (Gibco, 14190094) for 20 min at 4°C. Then lysates were centrifuged 20 min at 20000 x g. Supernatants were collected and mixed with TCEP (Thermo Scientific, 20490) and LDS NuPAGE (Thermo Scientific, NP0007) following manufacturer's instructions. Samples were boiled at 90°C for 5 min. Proteins were quantified according to Bradford assay were loaded on 10% SDS-PAGE gels (Bio-Rad, NP03006) or 15% for LC3 blot. Transfers were performed on Amersham Hybond 0.2 µm PVDF membrane (GE, RPN1520). Primary antibodies were incubated in PBS 0.5% Tween, 5% milk overnight. Secondary antibodies were incubated 1h15 at room temperature. Western blot detection was performed using Amersham ECL (GE, 28980926) on LAS 4000 camera (GE).

### ***Measles virus strain and infections***

Edmonston VR-24 measles virus strain from ATCC was used for all infections. The virus was diluted at the indicated multiplicity of infection in 500  $\mu$ l of DMEM, vigorously vortexed and put in contact with cells for 1.5 h. Then, 500  $\mu$ l of DMEM was added and cells were cultured for 48 h before further analysis. Eventually, *Salmonella* infection was performed at 42 h post MeV infection.

### ***Bacterial infection and gentamycin protection assay (CFU)***

*Salmonella enterica* serovar *typhimurium* 12023 (WT) or *sifA* mutant strains were grown in LB broth media for infections. Cell medium was changed for DMEM without antibiotics at least 24 h before infection. *Salmonella* was grown overnight in LB. The day of the infection, overnight culture was diluted at 1:33 in LB until the bacterial culture reaches an optical density of 0.15. Then, the culture was diluted at 1:10 in DMEM and cells were infected with 200  $\mu$ l (24 wells plate) or 800  $\mu$ l (6 wells plate) of *Salmonella* preparation for 15 min at 37°C. Cells were then washed twice in PBS and cultured in DMEM 10% FBS, 100  $\mu$ g/ml gentamycin for 1 h in order to kill extracellular bacteria. The medium was replaced for DMEM 10% FBS, 20  $\mu$ g/ml gentamycin until the end of the infection. The procedures used for infection of HeLa cells with *Shigella flexneri* was identical to that for infection with *Salmonella* except that the time of contact for infection was 1 h instead of 15 min. At the time point of interest (2 h, 4 h or 6 h), culture medium was removed from cell culture. Cells were washed twice in PBS and then permeabilized with 1 ml of 1% saponin (Sigma, S7900) for 10 min. Saponin preparation was homogenized and diluted at 1:10 and 1:100 in PBS (2 h and 4 h) or 1:100 and 1:1000 (6 h). 100  $\mu$ l of dilution were plated on LB agar plate and cultured overnight at 37°C. CFU were determined using the formula: (number of colonies\*dilution\*100).

### ***Confocal microscopy***

Infected or uninfected cells were first plated on glass slices and fixed with 2% paraformaldehyde diluted in PBS for 15 min at room temperature. Cells were permeabilized in 0.1% Triton solution for 5 min. Primary antibodies were incubated overnight in staining buffer (5% goat serum, 3% human serum, 1% BSA, PBS). Then, secondary antibodies were incubated for 75 min at room temperature in staining buffer). Nuclei were labeled with NucBlue (Invitrogen, R37606). Slices were mounted using Fluoromount (Agilent, S302380-2). All images were taken on LSM710 confocal microscope (Zeiss) with a 40X plan apochromat objective. Image analysis was performed using ImageJ software. The

number of syncytial bacteria was derived from a plan section by counting bacteria within syncytia until the value associated to 100 nuclei was obtained (typically, 25 to 30 syncytia counted). Two slides were counted. The number of bacteria was then normalized per nucleus.

### *Statistical analysis*

The p values were calculated using a two-tailed Welch t test (Student's t test assuming non-equal variances of the samples) except for CFU assays (paired Student t test) and western blot results (Wilcoxon test).

### **ACKNOWLEDGMENTS**

We thank Drs Y. Yanagi and T. Henry and for providing us with CD150, MeV-F and MeV-H-encoding vector, and *S. Typhimurium* and *S. flexneri* strains, respectively, as well as the imagery PLATIM and the flow cytometry facilities of the SFR Biosciences Gerland. This work was supported by Fondation pour la Recherche Médicale (Label FRM DEQ20170336729), ANR-14-CE14-0022 and Association François Aupetit (AFA). We thank Colombar Aldebert for technical help with WB fig 4C. We also thank Maud Michelet (CRCL), Anaëlle Dubois (CRCL), Jennifer Molle (CRCL), Sarah Heintz (CRCL) Caroline Pons (CIRI) and Emilie Charles (CIRI) for help with the isolation of primary human hepatocytes, as well as the staff from Prof Michel Rivoire's surgery room (CLB) for providing us with liver resections. We acknowledge the framework of the LABEX ECOFECT (ANR-11-LABX-0042) of Université de Lyon operated by the French National Research Agency (ANR-11-IDEX-0007), within which this work was performed.

### *Disclosure statement*

No potential conflict of interest.

### **REFERENCES**

1. Yang, Z., Klionsky, DJ. Eaten alive: a history of macroautophagy. *Nat Cell Biol* 2010; **12**: 814–822.

2. Mizushima, N., Yoshimori, T., Ohsumi, Y. The Role of Atg Proteins in Autophagosome Formation. *Annual Review of Cell and Developmental Biology* 2011; **27**: 107–132.
3. Stolz, A., Ernst, A., Dikic I. Cargo recognition and trafficking in selective autophagy. *Nature Cell Biology* 2014; **16**: 495–501.
4. Kirkin, V., Rogov, VV. A Diversity of Selective Autophagy Receptors Determines the Specificity of the Autophagy Pathway. *Molecular Cell* 2019; **76**: 268–285.
5. Bento, CF., *et al.* Mammalian Autophagy: How Does It Work? *Annual Review of Biochemistry* 2016; **85**: 685–713.
6. Levine, B., Mizushima, N., Virgin, HW. Autophagy in immunity and inflammation. *Nature* 2011; **469**: 323–335.
7. Huang, J., Brumell JH. Bacteria–autophagy interplay: a battle for survival. *Nature Reviews Microbiology* 2014; **12**: 101–114.
8. Paul, P., Münz, C. Autophagy and Mammalian Viruses. In: *Advances in Virus Research*. Elsevier, 2016, pp 149–195.
9. Viret, C., Duclaux-Loras, R., Nancey, S., Rozières, A., Faure, M. Selective Autophagy Receptors in Antiviral Defense. *Trends in Microbiology* 2021; **29**: 798–810.
10. Joubert, P.E., *et al.* Autophagy induction by the pathogen receptor CD46. *Cell Host Microbe* 2009; **6**: 354–366.
11. Richetta, C., *et al.* Sustained Autophagy Contributes to Measles Virus Infectivity. *PLoS Pathogens* 2013; **9**: e1003599.
12. Grégoire, IP., *et al.* IRGM Is a Common Target of RNA Viruses that Subvert the Autophagy Network. *PLoS Pathogens* 2011; **7**: e1002422.
13. Delpeut, S., Rudd, P.A., Labonté, P., von Messling, V. Membrane Fusion-Mediated Autophagy Induction Enhances Morbillivirus Cell-to-Cell Spread. *Journal of Virology* 2012; **86**: 8527–8535.
14. Rozières, A., Viret, C., Faure, M. Autophagy in Measles Virus Infection. *Viruses* 2017; **9**: 359.
15. Petkova, D., *et al.* Distinct Contributions of Autophagy Receptors in Measles Virus Replication. *Viruses* 2017; **9**: 123.

16. Birmingham, CL., *et al.* Autophagy Controls Salmonella Infection in Response to Damage to the Salmonella-containing Vacuole. *Journal of Biological Chemistry* 2006; **281**: 11374–11383.
17. Thurston, T.L.M., *et al.* The TBK1 adaptor and autophagy receptor NDP52 restricts the proliferation of ubiquitin-coated bacteria. *Nat Immunol* 2009; **10**: 1215–1221.
18. Zheng, Y.T., *et al.* The Adaptor Protein p62/SQSTM1 Targets Invading Bacteria to the Autophagy Pathway. *J Immunol* 2009; **183**: 5909–5916.
19. Wild, P., *et al.* Phosphorylation of the Autophagy Receptor Optineurin Restricts Salmonella Growth. *Science* 2011; **333**: 228–233.
20. Thurston, T.L.M., *et al.* Galectin 8 targets damaged vesicles for autophagy to defend cells against bacterial invasion. *Nature* 2012; **482**: 414–418.
21. Tumbarello, D.A., *et al.* The Autophagy Receptor TAX1BP1 and the Molecular Motor Myosin VI Are Required for Clearance of Salmonella Typhimurium by Autophagy. *PLOS Pathogens* 2015; **11**: e1005174.
22. Xia, M., *et al.* Mitophagy Enhances Oncolytic Measles Virus Replication by Mitigating DDX58/RIG-I-Like Receptor Signaling. *Journal of Virology* 2014; **88**: 5152–5164.
23. Herschke, F., *et al.* Cell-Cell Fusion Induced by Measles Virus Amplifies the Type I Interferon Response. *J Virol* 2007; **81**: 12859–12871.
24. Brumell, J.H., Tang, P., Zaharik, M.L., Finlay, BB. Disruption of the Salmonella-Containing Vacuole Leads to Increased Replication of *Salmonella enterica* Serovar Typhimurium in the Cytosol of Epithelial Cells. *Infect Immun* 2002; **70**: 3264–3270.
25. Stein, M.A., *et al.* Identification of a Salmonella virulence gene required for formation of filamentous structures containing lysosomal membrane glycoproteins within epithelial cells. *Mol Microbiol* 1996; **20**: 151–164.
26. Beuzon, C.R. Salmonella maintains the integrity of its intracellular vacuole through the action of SifA. *The EMBO Journal* 2000; **19**: 3235–3249.
27. Richter, B., *et al.* Phosphorylation of OPTN by TBK1 enhances its binding to Ub chains and promotes selective autophagy of damaged mitochondria. *Proceedings of the National Academy of Sciences* 2016; **113**: 4039–4044.

28. Rogov, V.V., *et al.* Structural basis for phosphorylation-triggered autophagic clearance of Salmonella. *Biochemical Journal* 2013; **454**: 459–466.
29. Clark, K., Plater, L., Peggie, M., Cohen, P. Use of the Pharmacological Inhibitor BX795 to Study the Regulation and Physiological Roles of TBK1 and I $\kappa$ B Kinase  $\epsilon$ . *Journal of Biological Chemistry* 2009; **284**: 14136–14146.
30. Klionsky, D.J., *et al.* Guidelines for the use and interpretation of assays for monitoring autophagy (4th edition) <sup>1</sup>. *Autophagy* 2021; **17**: 1–382.
31. Katsuragi, Y., Ichimura, Y., Komatsu, M. p62/SQSTM1 functions as a signaling hub and an autophagy adaptor. *FEBS J* 2015; **282**: 4672–4678.
32. Sánchez-Martín, P., Komatsu, M. p62/SQSTM1 – steering the cell through health and disease. *Journal of Cell Science* 2018; **131**: jcs222836.
33. Sagnier, S., *et al.* Autophagy Restricts HIV-1 Infection by Selectively Degrading Tat in CD4<sup>+</sup> T Lymphocytes. *Journal of Virology* 2015; **89**: 615–625.
34. Birgisdottir, Á.B., Lamarkn, T., Johansen, T. The LIR motif – crucial for selective autophagy. *Journal of Cell Science* 2013; **126**: 3237–3247.
- 35- Lobato-Márquez D., *et al.* A requirement for septins and the autophagy receptor p62 in the proliferation of intracellular Shigella. *Cytoskeleton* 2019; **76**:163-172.
36. Gomes, L.C., Dikic, I. Autophagy in Antimicrobial Immunity. *Molecular Cell* 2014; **54**: 224–233.
37. Kohler, L.J., Roy, C.R. Autophagic targeting and avoidance in intracellular bacterial infections. *Current Opinion in Microbiology* 2017; **35**: 36–41.
38. Choi, Y., Bowman, J.W., Jung, J.U. Autophagy during viral infection — a double-edged sword. *Nature Reviews Microbiology* 2018; **16**: 341–354.
39. Cemma, M., Kim, P.K., Brumell, J.H. The ubiquitin-binding adaptor proteins p62/SQSTM1 and NDP52 are recruited independently to bacteria-associated microdomains to target Salmonella to the autophagy pathway. *Autophagy* 2011; **7**: 341–345.
40. Kishi-Itakura C., *et al.* Ultrastructural insights into pathogen clearance by autophagy. *Traffic* 2020; **4**:310-323



41. von Muhlinen, N., *et al.* LC3C, Bound Selectively by a Noncanonical LIR Motif in NDP52, Is Required for Antibacterial Autophagy. *Molecular Cell* 2012; **48**: 329–342.
42. Verlhac, P., *et al.* Autophagy Receptor NDP52 Regulates Pathogen-Containing Autophagosome Maturation. *Cell Host & Microbe* 2015; **17**: 515–525.
43. Ravenhill, B.J., *et al.* The Cargo Receptor NDP52 Initiates Selective Autophagy by Recruiting the ULK Complex to Cytosol-Invading Bacteria. *Molecular Cell* 2019; **74**: 320-329.e6.
44. Turco, E., *et al.* FIP200 Claw Domain Binding to p62 Promotes Autophagosome Formation at Ubiquitin Condensates. *Molecular Cell* 2019; **74**: 330-346.e11.
45. Matsumoto, G., Shimogori, T., Hattori, N., Nukina, N. TBK1 controls autophagosomal engulfment of polyubiquitinated mitochondria through p62/SQSTM1 phosphorylation. *Hum Mol Genet* 2015; **24**: 4429–4442.
46. Schlütermann, D., *et al.* FIP200 controls the TBK1 activation threshold at SQSTM1/p62-positive condensates. *Sci Rep* 2021; **11**: 13863.
47. Noad, J., *et al.* LUBAC-synthesized linear ubiquitin chains restrict cytosol-invading bacteria by activating autophagy and NF- $\kappa$ B. *Nat Microbiol* 2017; **2**: 17063.
48. van Wijk, S.J.L., *et al.* Linear ubiquitination of cytosolic Salmonella Typhimurium activates NF- $\kappa$ B and restricts bacterial proliferation. *Nat Microbiol* 2017; **2**: 17066.
49. Pattingre, S., *et al.* Bcl-2 Antiapoptotic Proteins Inhibit Beclin 1-Dependent Autophagy. *Cell* 2005; **122**: 927–939.
50. Lee, J.S., *et al.* FLIP-mediated autophagy regulation in cell death control. *Nat Cell Biol* 2009; **11**: 1355–1362.
51. Campbell, G.R., Rawat, P., Bruckman, R.S., Spector, S.A. Human Immunodeficiency Virus Type 1 Nef Inhibits Autophagy through Transcription Factor EB Sequestration. *PLoS Pathog* 2015; **11**: e1005018.
52. Beale, R., *et al.* A LC3-Interacting Motif in the Influenza A Virus M2 Protein Is Required to Subvert Autophagy and Maintain Virion Stability. *Cell Host & Microbe* 2014; **15**: 239–247.
53. Zhou, Z., *et al.* Autophagy is involved in influenza A virus replication. *Autophagy* 2009; **5**: 321–328.

54. Reggiori, F., *et al.* Coronaviruses Hijack the LC3-I-Positive EDEMosomes, ER-Derived Vesicles Exporting Short-Lived ERAD Regulators, for Replication. *Cell Host & Microbe* 2010; **7**: 500–508.
- 55- Kreibich S., *et al.* Autophagy Proteins Promote Repair of Endosomal Membranes Damaged by the Salmonella Type Three Secretion System 1. *Cell Host Microbe* 2015; **18**:527-37.
- 56- Lobato-Márquez D., *et al.* A requirement for septins and the autophagy receptor p62 in the proliferation of intracellular Shigella. *Cytoskeleton* 2019; **76**:163-172.
57. Bell, L.C.K., Noursadeghi, M. Pathogenesis of HIV-1 and Mycobacterium tuberculosis co-infection. *Nat Rev Microbiol* 2018; **16**: 80–90.
58. Sharma, V., *et al.* Trehalose limits opportunistic mycobacterial survival during HIV co-infection by reversing HIV-mediated autophagy block. *Autophagy* 2021; **17**: 476–495.
59. Griffin, D.E. Measles virus-induced suppression of immune responses: Measles virus-induced immunosuppression. *Immunological Reviews* 2010; **236**: 176–189.
60. Moss, W.J. Measles. *The Lancet* 2017; **390**: 2490–2502.
61. Lecluyse S.E., *et al.* Isolation and culture of primary hepatocytes from resected human liver tissue. *Methods Mol Biol* 2010; **640** 57-82

## LEGENDS TO FIGURES

**Figure 1.** *S. Typhimurium* hyper-replicates in measles virus co-infected syncytial cells. **(A)** HeLa cells cultured with or without MeV for 42 h were then infected with *S. Typhimurium* during 6 h prior to western blot analysis for LC3, the nucleoprotein of MeV (MeV-N) and ACTB/ $\beta$ -ACTIN. The signals of the displayed blot were quantified, and the values represent the amount of LC3-II normalized to ACTB. MOI=multiplicity of infection. Values represent the mean  $\pm$  SD of 3 independent experiments. ns: not significant, \* $p$ <0.05. **(B)** HeLa cells were infected with *S. Typhimurium* only or together with MeV as in **(A)** prior to gentamicin protection assay. Values of colony forming units (CFU) were used to derive the fold expansion of bacteria between 2 and 6 h of infection and data were normalized to cultures infected with *S. Typhimurium* only. Values represent the mean  $\pm$  SD of 3 independent experiments. \* $p$ <0.05. **(C)** HeLa cells infected during 6 h with *S. Typhimurium* after a previous 48 h culture with or without MeV were stained for intracellular bacteria (red), MeV-N (green) and nuclei (blue) prior to analysis by confocal microscopy. Areas from co-infected cells enriched in either mono-nucleated or syncytial (white dotted contours) cells, were photographed separately. Representative images are shown accompanied with a graph of the quantified average number of bacteria per nucleus. Values represent the mean  $\pm$  SD of 3 independent experiments. ns: not significant, \*\* $p$ <0.01, \*\*\*\* $p$ <0.0001. **(D)** HeLa cells were infected during 2, 4 or 6 h with *S. Typhimurium* within the last 48 h culture with or without MeV and stained as in **(C)**. The averages of the absolute number of *S. Typhimurium* per nucleus were quantified at each time point and represented as histograms. Values represent the mean  $\pm$  SD of 3 independent experiments. ns: not significant, \*\*\*\* $p$ <0.0001. **(E)** HeLa cells treated with FIP or DMSO (vehicle) were infected as in **(C)** prior to gentamicin protection assay and a 6 h:2 h ratio of bacterial CFU was derived to represent the bacterial load in virus/bacteria co-infected cultures relative to cultures treated with DMSO and infected with *S. Typhimurium* only. This experiment was carried out once. **(F)** HeLa cells cultured in the presence of the fusion inhibitory peptide (FIP) were infected as in **(B)** and stained as in **(C)** prior to confocal microscopy analysis. Representative images are shown (white dotted contours are syncytia)

along with a quantification of the average number of *S. Typhimurium* per nucleus. Values represent the mean of 2 independent experiments.

**Figure 2.** *S. Typhimurium* cells that hyper-replicates within MeV-induced syncytia are essentially cytosolic and ubiquitinated, yet do not colocalize with autophagosomes. **(A)** HeLa cells were infected and cultured as in Figure 1C (MOI 0.03), stained for intracellular bacteria (red), LAMP1 (green) and nuclei (blue), and analyzed by confocal microscopy. The *sifA* mutant strain (*sifA*) was used in parallel to regular *S. Typhimurium* (WT). Representative images of each culture are shown (white dotted contours delineate syncytia), accompanied with histograms showing the relative frequency of *S. Typhimurium* that colocalized with LAMP1. Values represent the mean  $\pm$  SD of 3 independent experiments. The scale bar represents 50  $\mu$ m. ns: not significant, \* $p < 0.05$ , \*\* $p < 0.01$ . **(B)** Transmission Electronic microscopy analysis of HeLa cells after 6 h of infection with regular *S. Typhimurium* (WT) only (top line), the *sifA* mutant strain only (bottom line) or, with both MeV and regular *S. Typhimurium* (middle line). Representative images are shown. The black arrow indicates a vacuolar membrane surrounding bacteria in cells infected with WT bacteria only. This experiment was carried out once. **(C)** HeLa cells stably expressing a GFP-LC3 reporter construct (green) were infected with MeV (MOI 0.3) for 48 h and infected with *S. Typhimurium* during the last 6 h of culture. Cells were stained for intracellular bacteria (red), ubiquitin (white) and nuclei (blue), and analyzed by confocal microscopy. Representative images depicting bacterial patches within syncytia are shown. Unlike very rare bacteria that appears to be efficiently targeted by the autophagy machinery (white arrow), a majority of bacteria failed to recruit GFP-LC3, despite efficient ubiquitination. Images are accompanied by histograms showing the relative frequency of *S. Typhimurium* that colocalized with either ubiquitin, LC3, both ubiquitin and LC3, or that lacked both markers (negative), in virus/bacteria co-infected syncytia. Values represent the mean  $\pm$  SD of 3 independent experiments. The scale bar represents 50  $\mu$ m. \*\*\* $p < 0.001$ .

**Figure 3.** *S. Typhimurium* replication in MeV-induced syncytia is insensitive to TBK-1 engagement and autophagic activity. **(A)** HeLa cells were cultured as in **Figure 1C** (MOI 0.03) in the presence of the TBK1 inhibitor BX795 or vehicle (DMSO) and stained for intracellular bacteria (red), MeV-N protein (green) and nuclei (blue) prior to analysis by confocal microscopy. Representative images with delineated syncytia (white dotted lines) are shown. Histograms indicating the average number of bacteria per nucleus were derived as in Figure 1C. Values represent the mean +/- SD of 3 independent experiments. The scale bar represents 50  $\mu\text{m}$ ; ns: not significant, \*\* $p < 0.01$ . **(B)** HeLa cells treated with the indicated siRNA were cultured as in **(A)** and stained for intracellular bacteria (red), MeV-N (green) and nuclei (blue) prior to analysis by confocal microscopy. Representative images with delineated syncytia (white dotted lines) are shown. Histograms indicating the average number of bacteria per nucleus were derived as in Figure 1C. Values represent the mean of 2 independent experiments. The scale bar represents 50  $\mu\text{m}$ . **(C)** HeLa cells treated with siRNAs targeting the core autophagy factors ATG5 and ATG7 were infected with MeV (MOI 0.03) during 48 h, infected with *S. Typhimurium* for the last 6 h, processed for intracellular staining of bacteria (red), MeV-N (green), and nuclei (blue) and analyzed by confocal microscopy. Representative images with delineated syncytia (white dotted lines) are shown. Histograms indicating the average number of bacteria per nucleus were derived as in Figure 1C. Values represent the mean +/- SD of 3 independent experiments. The scale bar represents 50  $\mu\text{m}$ ; ns: not significant.

**Figure 4.** MeV infection is associated with a lowered expression level of autophagy receptor SQSTM1 and TAX1BP1 that is maintained upon coinfection with *S. Typhimurium*. **(A)** HeLa cells cultured with or without MeV were infected with *S. Typhimurium* for 6 h prior to western blot analysis for SQSTM1, MeV-N and ACTB expression. The signals of the displayed blot were quantified by densitometry and the values represent the ACTB-normalized level of SQSTM1 for the different conditions relative to uninfected cells. Histograms represent the mean +/- SD of 3 independent experiments. ns: not significant, \* $p < 0.05$ , \*\* $p < 0.01$ . Note that the displayed western blot image corresponds to the same membrane as in Figure 1A but blotted for SQSTM1. **(B)** Autophagy

receptor expression level in MeV infected (MOI 0.1) and control, HeLa cells. CALCOCO2, OPTN, TAX1BP1, SQSTM1 and ACTB levels were analyzed by western blot and quantified. A representative image is shown. Values represent the mean  $\pm$  SD of the autophagy receptor:ACTB ratio normalized to control cells for 3 independent experiments. ns: not significant,  $^{***}p<0.01$ . (C) HeLa cell cultures were kept uninfected or infected with either MeV (MOI 0.03) or MeV plus *S. Typhimurium*. Similar cultures were separately treated with bafilomycin A<sub>1</sub> (BAFA1) or the proteasomal inhibitor MG132 (vs vehicle for uninfected cells). Western blot analyses were performed for SQSTM1, TAX1BP1, LC3 and GAPDH. Histograms represent quantification values for SQSTM1, TAX1BP1 and the LC3-II:LC3-I ratio normalized to GAPDH. Values represent the mean  $\pm$  SD of 3 independent experiments.  $^{*}p<0.05$ ,  $^{**}p<0.01$ .

**Figure 5.** Ensuring a constitutive expression level of SQSTM1 and TAX1BP1 autophagy receptors in MeV-infected cells restores their anti-*Salmonella* autophagic capacity. (A) HeLa cells transfected with expression vectors carrying SQSTM1 or TAX1BP1 cDNAs were infected with MeV (MOI 0.1) for 48 h and coinfecting or not with *S. Typhimurium* during the last 6 h prior to gentamycin protection assay. CFU values were used to derive the bacteria fold expansion between 2 and 6 h of infection. Values represent the mean  $\pm$  SD of 3 independent experiments. (B and C) HeLa cells transfected with the indicated cDNAs were infected with MeV (MOI 0.03) for 48 h and coinfecting with *S. Typhimurium* during the last 6 h prior to immuno-staining for intracellular bacteria (red) and nuclei (blue), and analysis by confocal microscopy. Representative images with delineated syncytia are shown. Histograms represent the average number of bacteria per nucleus. Values represent the mean of 2 independent experiments (B) and the mean  $\pm$  SD of 3 independent experiments (C). The scale bar represents 50  $\mu$ m; ns: not significant,  $^{*}p<0.05$ . (D and E) HeLa cells expressing GFP-LC3 were processed as in B and C and immuno-stained for intracellular bacteria, LAMP1 and nuclei. Representative images with delineated syncytia are shown. Histograms represent the relative frequency of bacteria positive for LC3 (D) or LAMP1 (E). Values represent the mean of 2 independent experiments. The scale bar represents 50  $\mu$ m.

**Figure 6.** MeV infection conditions human primary epithelial cells for *S. Typhimurium* cytosolic hyperproliferation and renders HeLa cells more resistant to *S. flexneri* intracellular growth. **(A)** Human primary epithelial cells from liver biopsies were maintained in culture for 6 days, infected or not with MeV (MOI 0.03) for 48 h and coinfecting *S. Typhimurium* with during the last 6 h prior to gentamycin protection assay. CFU values obtained after 2 and 6 h of infection were used to derive a fold replication index for both culture conditions. Cells obtained from two donors were analyzed in independent experiments. **(B)** Human primary hepatocytes from one donor (#2) were prepared as in **(A)**, immuno-stained for bacteria (red) and nuclei (blue) and analyzed by confocal microscopy. Representative images are shown. The histograms represent the mean of the number of bacteria per nucleus. **(C)** Western blot analysis of SQSTM1 and ACTB expression by human primary hepatocytes (PHH) from one donor (#1) after infection with MeV for 48 h and coinfection with *S. Typhimurium* during the last 6 h. Histograms represent the amount of SQSTM1 relative to ACTB and normalized to the uninfected control. **(D)** HeLa cell cultures were kept uninfected or infected with MeV (MOI 0.03) for 48 h prior to *S. flexneri* infection during the last 6 h and gentamycin protection assay. CFU values obtained after 2 and 6 h of infection were used to derive a fold replication index for both conditions. The histograms represent the mean  $\pm$  SD of 3 independent experiments. \*\* $p < 0.01$ .

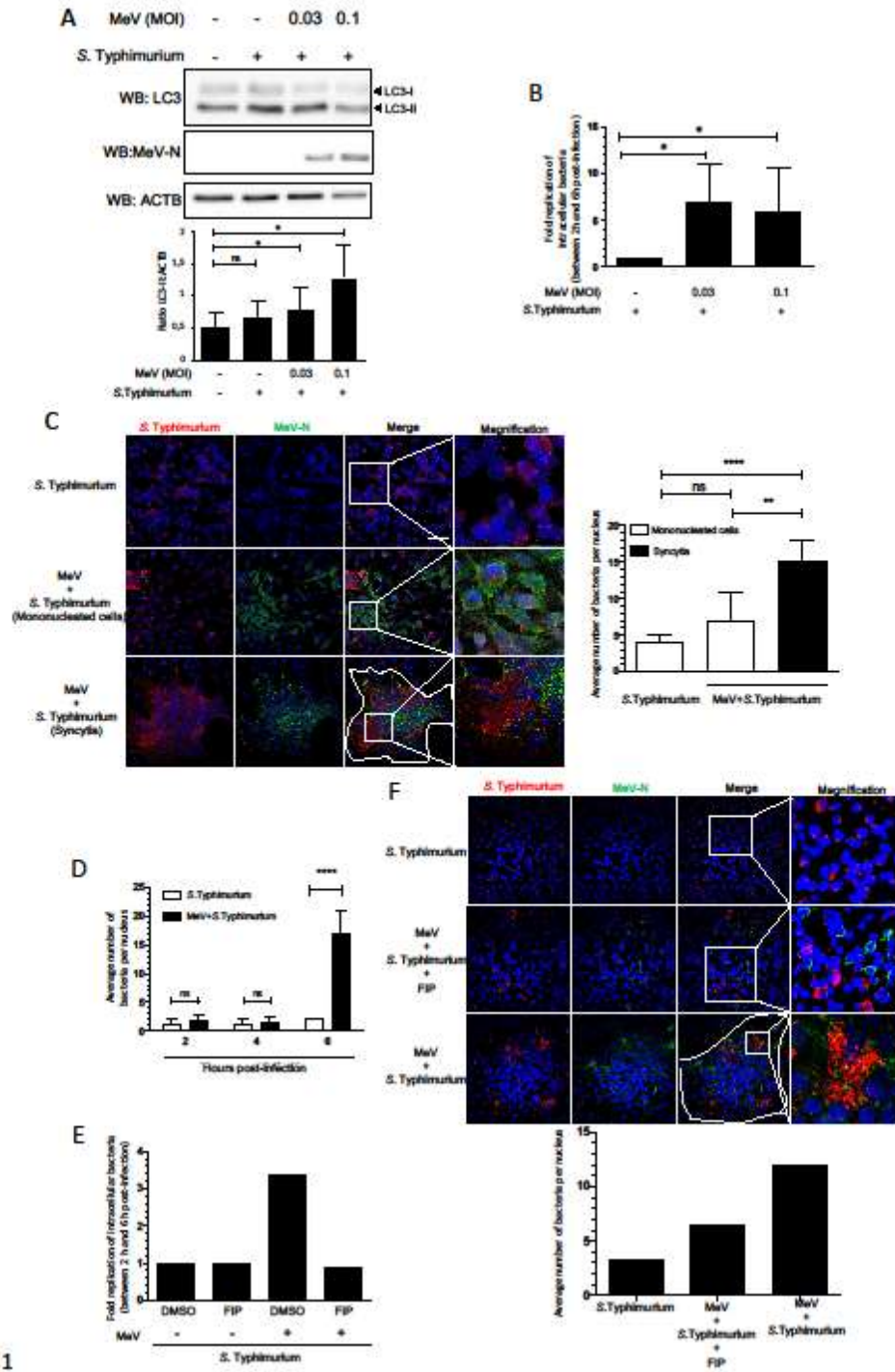


Figure 1



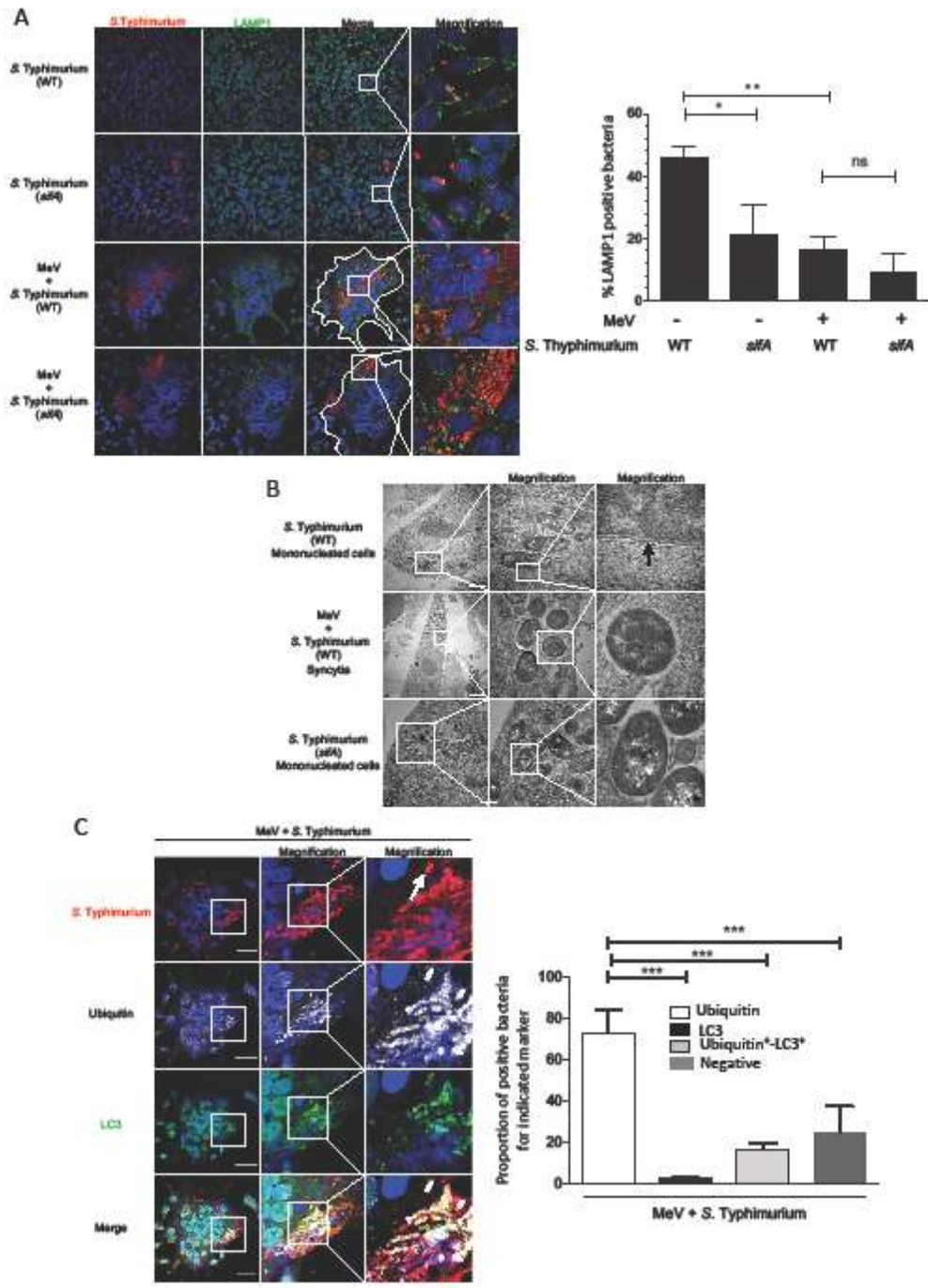


Figure 2

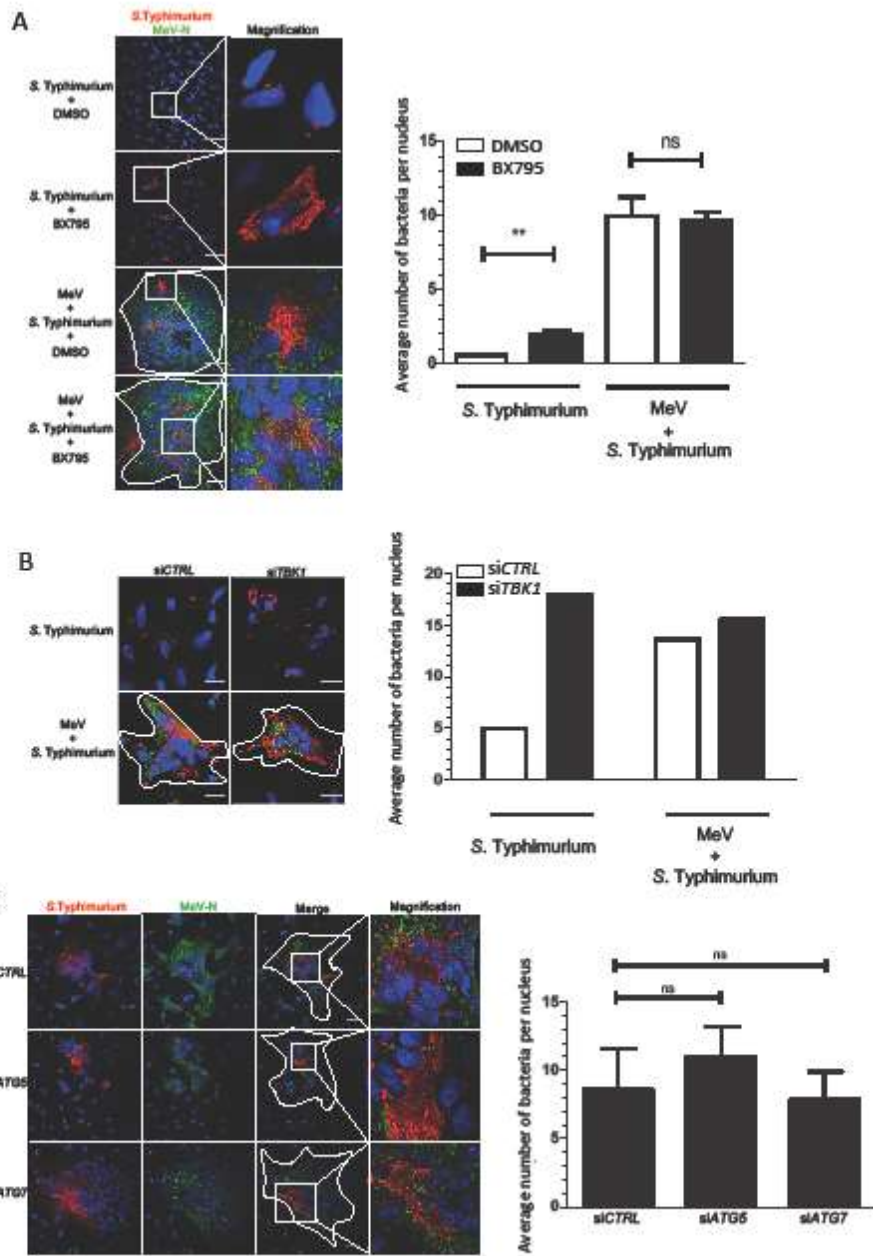


Figure 3

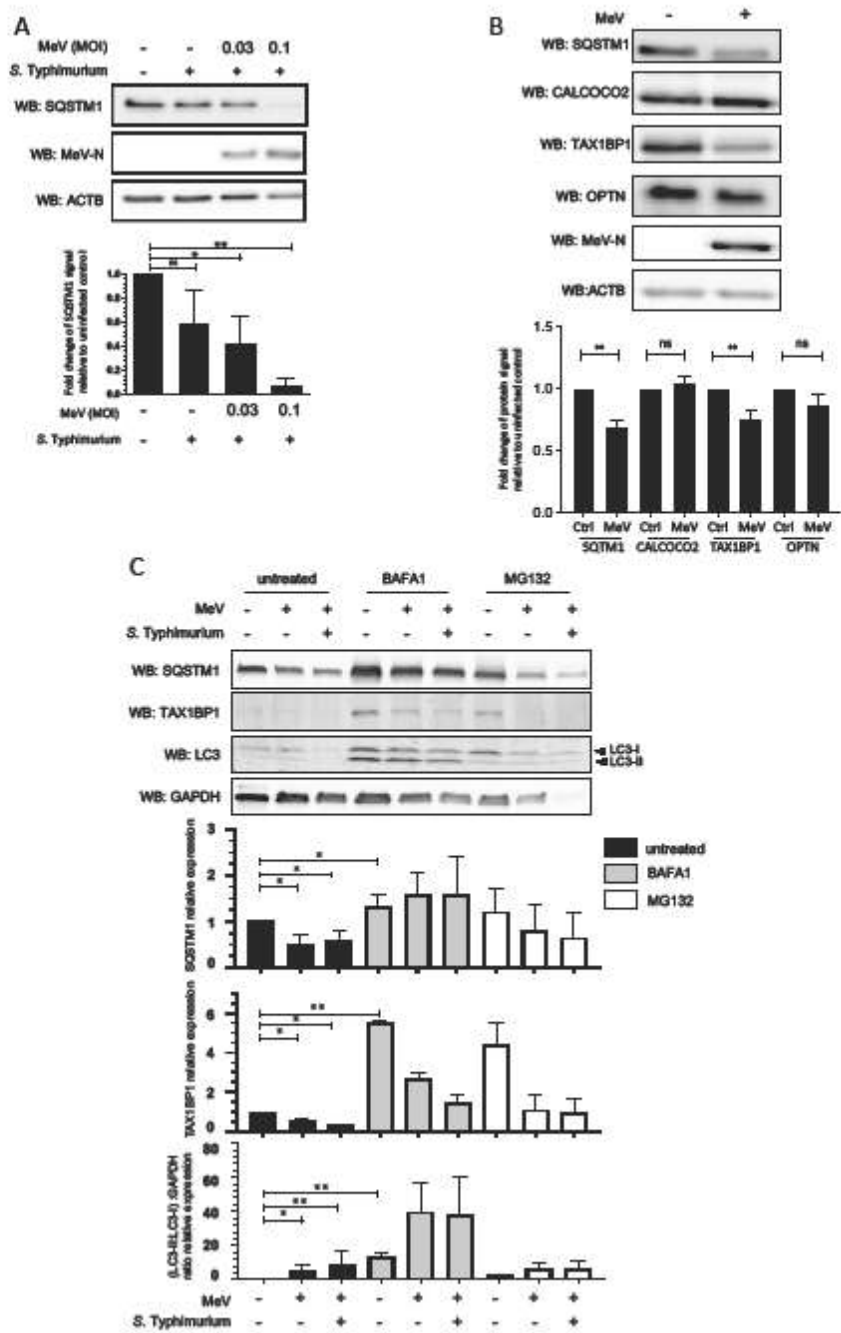


Figure 4

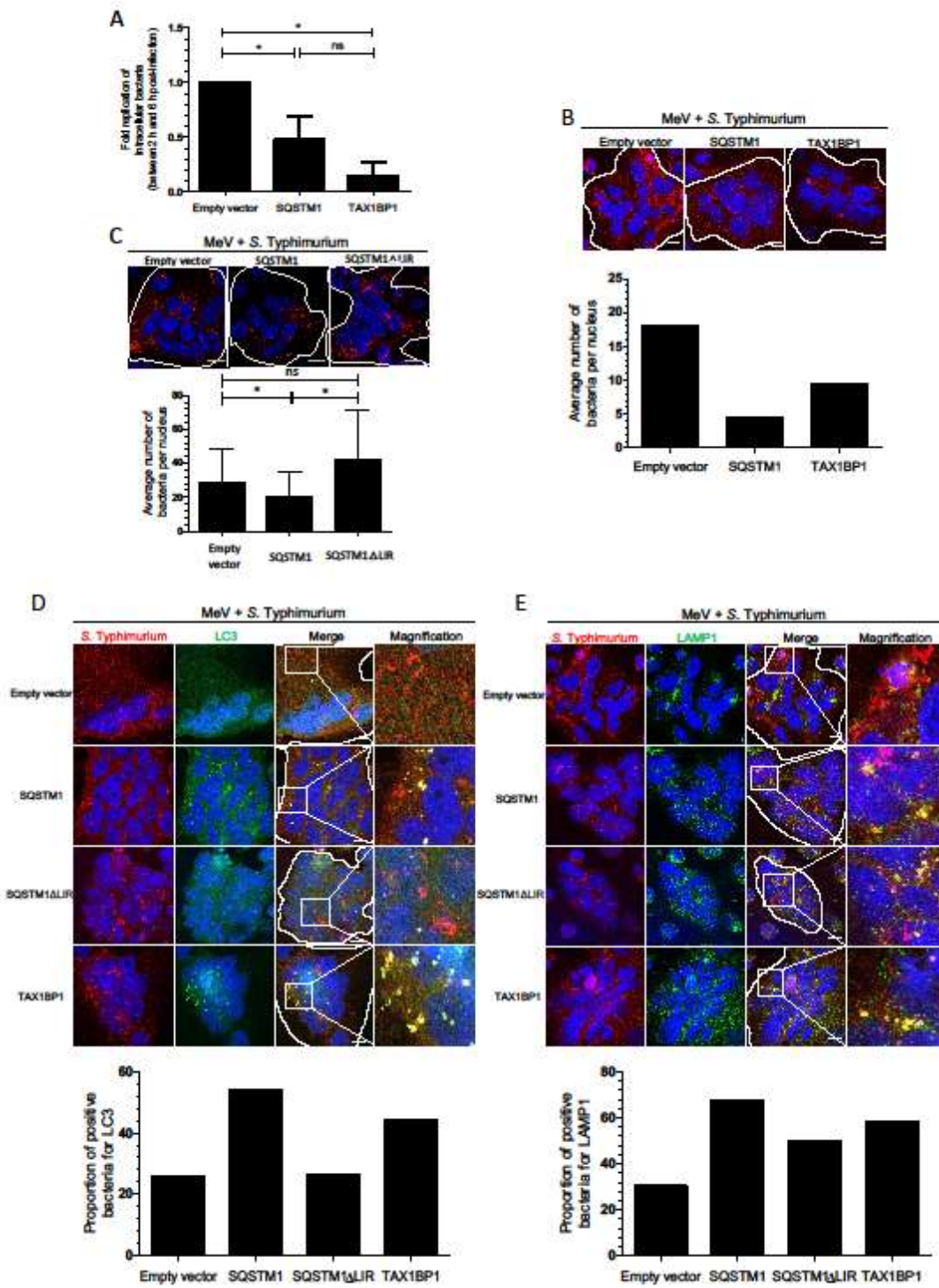


Figure 5

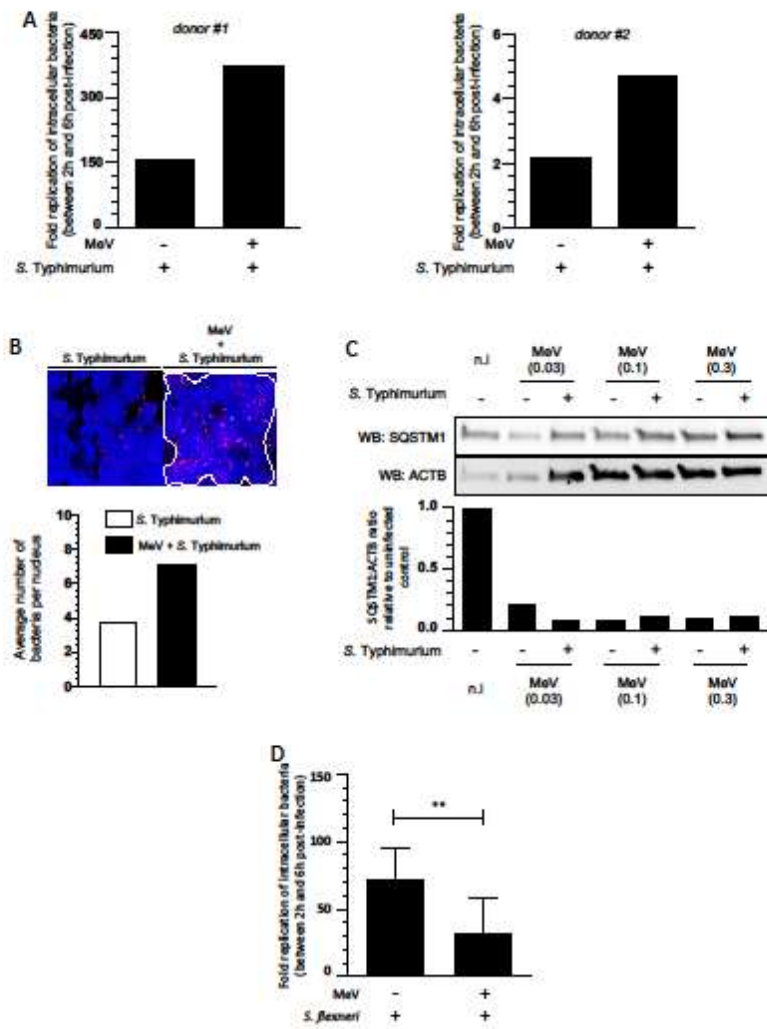


Figure 6